

# EagleVision: A Dual-Stage Framework with BEV-grounding-based Chain-of-Thought for Spatial Intelligence

Jiaxu Wan<sup>1</sup>, Xu Wang<sup>3</sup>, Mengwei Xie<sup>3</sup>, Hang Zhang<sup>3</sup>,

Mu Xu<sup>3</sup>, Yang Han<sup>2</sup>, Hong Zhang<sup>1</sup>, Ding Yuan<sup>1</sup>, Yifan Yang<sup>1,\*</sup>

<sup>1</sup>School of Aerospace, BUAA

<sup>2</sup>School of Software, BUAA

<sup>3</sup>Independent Researcher

## 1. Instruct MLLM:

Lack of Thinking

Which one is more near to **bed**?  
Chair or **Sofa**.

Sofa.



## 2. Thinking with Text:

Lack of Spatial Thinking

Which one is more near to **bed**?  
Chair or **Sofa**.

Oh, but I can't find the chair and sofa.

My answer is **sofa**.



## 3. EagleVision (Ours):

Two Stage for “Thinking with Space”

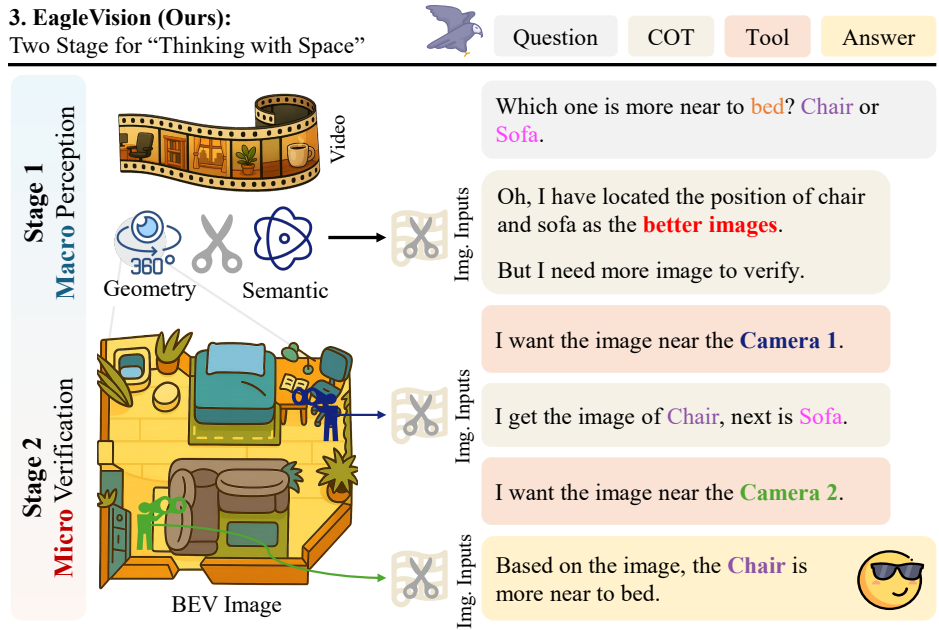


Figure 1. **Overview of EagleVision.** Compared with conventional instruction-following or text-only Chain-of-Thought (CoT) models that lack explicit spatial reasoning, EagleVision is a dual-stage framework for progressive spatial cognition through macro perception and micro verification. (1) Macro perception selects a compact yet spatially informative set of frames by jointly considering semantic relevance and geometric diversity under a token budget. (2) Micro verification formalize spatial multi-modal CoT as BEV-grounding based pose querying with a spatial reward for verifiable spatial observations, forming a verifiable evidence chain for interpretable, geometry-aware answers.

## Abstract

Recent spatial intelligence approaches typically attach 3D cues to 2D reasoning pipelines or couple MLLMs with black-box reconstruction modules, leading to weak spatial consistency, limited viewpoint diversity, and evidence chains that cannot be traced back to supporting views. Frameworks for “thinking with images” (e.g., ChatGPT-o3 and DeepEyes) show that stepwise multimodal reasoning can emerge by interleaving hypothesis formation with active acquisition of visual evidence, but they do not address three key challenges in spatial Chain-of-Thought (CoT): building global space perception under strict token budgets, explicitly associating 3D hypotheses with video frames for verification, and designing spatially grounded rewards for reinforcement learning. To address these issues, we present **EagleVision**, a dual-stage framework for progressive spatial cognition through macro perception and micro verifica-

tion. In the macro perception stage, EagleVision employs a semantics-perspective-fusion determinantal point process (SPF-DPP) to select a compact set of geometry- and semantics-aware keyframes from long videos under a fixed token budget. In the micro verification stage, we formalize spatial CoT as BEV-grounded pose querying: the agent iteratively predicts poses on a BEV plane, retrieves the nearest real frames, and is trained purely by reinforcement learning with a spatial grounding reward that scores the consistency between predicted poses and observed views. On VSI-Bench, EagleVision achieves state-of-the-art performance among open-source vision-language models, demonstrating strong and generalizable spatial understanding.

## 1. Introduction

Spatial intelligence [6, 8], including reasoning about geometry [15, 29, 33, 34], pose [32, 42], and motion across views [36, 41], is fundamental for embodied perception [11,

28] and multimodal understanding [3, 4, 44]. Despite the rapid progress of multimodal large language models (MLLMs) in image-level reasoning [10, 13, 19, 45, 47], many existing systems still treat 3D inputs as auxiliary context attached to 2D pipelines [6, 8, 17], or tightly couple MLLMs with explicit 3D reconstruction modules [12, 46, 48]. Such designs under-utilize space as an *active reasoning workspace*, making it difficult to select informative viewpoints or assemble verifiable multi-view evidence.

Recent agent-based Chain-of-Thought (CoT) models [16, 23, 27, 39, 47] suggest a different paradigm, where hypothesis development is interleaved with active acquisition and manipulation of visual evidence. The emerging methodology of “thinking with images” instantiates this idea at the image level. For example, ChatGPT-o3 [19] integrates images into the model’s internal CoT and uses tools to crop, zoom, rotate, and otherwise manipulate user-provided images while reasoning step-by-step. DeepEyes [47] further demonstrates that such interleaved multimodal CoT [13] can be learned end-to-end by reinforcement learning, without cold-start SFT, as agents learn to select visual tools, acquire intermediate evidence frames, and write back observations to refine hypotheses.

However, extension of this image-level paradigm to *spatial Chain-of-Thought (spatial CoT)* over spatial task introduces unique challenges. First, **token budgets conflict with global spatial coverage**. Spatial reasoning often requires broad baselines and rich parallax to resolve geometry, but naive temporal sampling over long videos tends to discard viewpoint diversity and semantic coverage, making it difficult to build a global mental map of the scene under a fixed token limit. Second, unlike manipulating a single image canvas, spatial reasoning requires an explicit and deterministic mechanism to **map video frames into a 3D space for verification**. Hypotheses about object locations and their relations must be expressed in a common global coordinate system and grounded by retrieving concrete frames that observe the queried poses, so that abstract 3D hypotheses can be systematically tested against real observations. Third, large-scale supervision for multi-step spatial CoT is scarce, and learning accurate pose-conditioned querying from answer-only labels is non-trivial. This calls for training schemes that **reward spatially grounded decisions** under tool use, rather than merely matching final answers.

To tackle these challenges, we propose **EagleVision**, a dual-stage framework for progressive spatial cognition through macro perception and micro verification. In the first stage, **macro perception** builds a compact yet globally informative evidence set via **SPF-DPP**, a semantics–perspective-fusion determinantal point process that jointly optimizes semantic importance and  $SE(3)$  viewpoint diversity under a fixed token budget. In the second stage, **micro verification** performs iterative BEV-grounded

chain-of-thought by allowing the agent to issue explicit pose-conditioned queries on the BEV plane. At each reasoning step, the agent can either generate text or predict a BEV pose, which is matched via a scale-aware metric to the nearest real frame and added as new evidence. We further introduce a spatial reward that reflects the reliability of BEV-grounded retrieval, encouraging the agent to maintain accurate BEV grounding and avoid repeatedly probing regions without camera coverage.

In general, our contributions are summarized as follows: (1) We introduce EagleVision, a dual-stage framework for progressive spatial cognition through macro perception and micro verification. (2) For macro perception, we propose **SPF-DPP**, a semantics–perspective-fusion DPP that selects a concise yet spatially diverse frame set by jointly modeling semantic relevance and 3D viewpoint diversity. (3) For micro verification, we operationalize **spatial CoT as BEV-based pose querying** and train the querying policy purely via reinforcement learning with a spatial grounding reward, without any CoT supervision. (4) On VSI-Bench [38], EagleVision achieves state-of-the-art performance among open-source VLMs, demonstrating strong spatial understanding and generalization.

## 2. Related Work

**Spatial-Intelligence MLLMs.** Recent studies on multimodal large language models (MLLMs) for spatial intelligence mainly follow two directions: (i) incorporating point-cloud representations [30, 40] into general-purpose multimodal models with task-specific instruction tuning [6, 9, 17, 22, 26, 46, 48], and (ii) integrating 3D reconstruction modules as geometric priors with instruction-aligned fine-tuning [8, 12, 31, 48]. In the first direction, SIG3D [22] discretizes scenes into voxels or points and introduces a context-aware estimator with QA head, underscoring the value of voxel-based representations for 3D spatial reasoning. ShapeLLM [26] improves the embodied interaction by coupling a 3D encoder with instruction data to improve the alignment of semantics, geometry and language. In the second direction, VLM-3R [12] takes advantage of spatial features from DUS3R [33] and fine-tunes curated datasets to improve spatial intelligence. In contrast, our work introduces a multimodal CoT framework that performs progressive reasoning across vision, geometry, and semantics, moving beyond the simple optimization of spatial features.

**Interleaved-Modal CoT.** Interleaved-Modal CoT (ICoT) [13] alternates visual evidence and textual reasoning within one rollout, enhancing vision–language alignment and interpretability. Closed-source systems like ChatGPT-o3 [23] show strong agentic CoT behaviors, including tool use and iterative refinement, but their spatial grounding remains opaque. DeepEyes [47] further explores tool-augmented multimodal reasoning, yet it is not

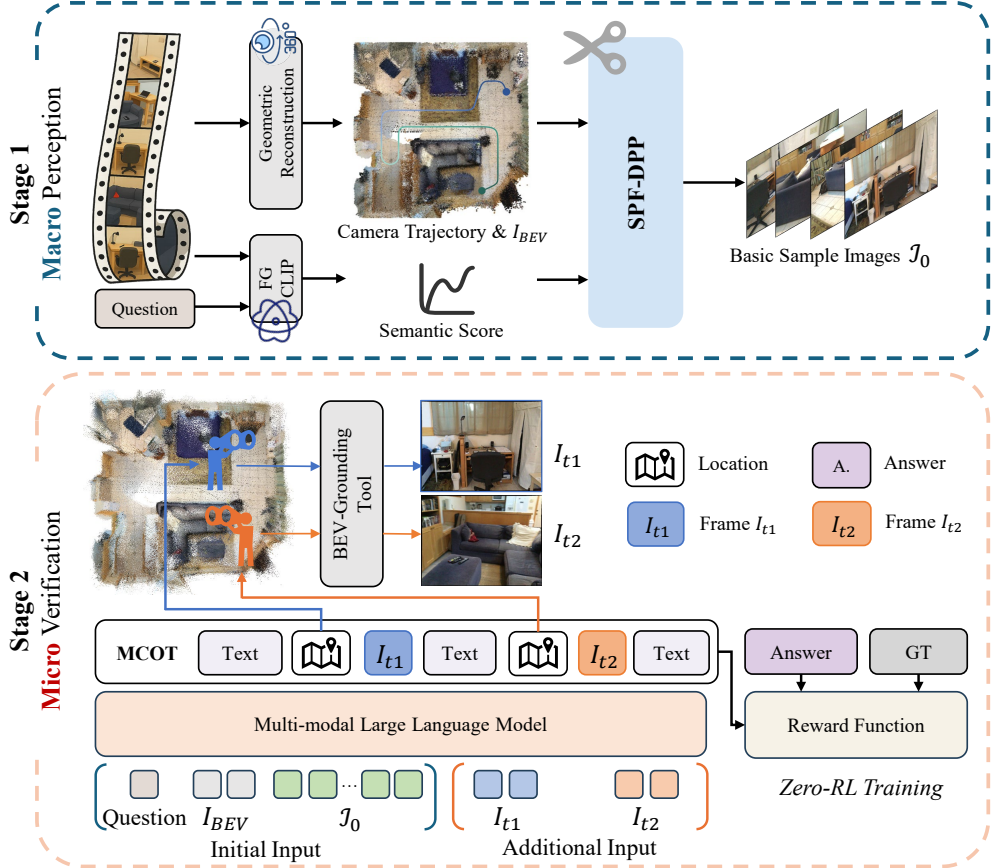


Figure 2. **Framework of EagleVision.** The framework consists of two stages for progressive spatial cognition: (i) Macro perception for selecting spatially informative frames under a token budget, and (ii) Micro verification with spatial thinking to refine spatial understanding.

designed for spatial intelligence. In contrast, our method explicitly targets spatial reasoning by interleaving vision, geometry, and semantics through BEV-based evidence and pose-aware tool calls, forming traceable chains that tightly couple visual and geometric cues.

### 3. Method

#### 4. Overall Architecture

**Framework Overview.** EagleVision is a dual-stage multimodal framework for spatial reasoning that leverages *macro perception* and *micro verification*. Unlike previous multimodal approaches that mainly perform image-level reasoning over 2D inputs for tasks such as object grounding or scene description, EagleVision targets inherently 3D spatial tasks that require understanding geometry, viewpoint relationships, and motion across video frames. The key idea is to decouple (i) macro perception for constructing a compact but geometry-aware evidence set from (ii) micro verification executing BEV-grounded Chain-of-Thought (CoT) reasoning with active view selection.

As illustrated in Fig. 2, EagleVision operates on top of an

explicit SLAM-based reconstruction backend rather than an end-to-end black-box 3D module. Given a video and a textual query, the *macro perception* stage selects a compact yet spatially informative subset of frames under a token budget, preserving key geometry while remaining query-relevant. The resulting keyframes, together with BEV projections of the reconstructed scene, provide a global spatial prior. The *micro verification* stage then performs iterative CoT reasoning, during which the model can either terminate with an answer or actively request additional views at specific BEV poses to refine its spatial understanding. Details of hyperparameters and implementation are provided in the supplementary material.

**Macro Perception.** Given an input video, we apply the SLAM-based system Vipe [18] to estimate per-frame camera poses and depth maps. Vipe follows a classical, fully interpretable SLAM pipeline rather than an end-to-end learned reconstruction module, and is used as a frozen pre-processing stage that supplies explicit geometric cues (poses and depth) to the reasoning model. The recovered poses and depths are projected onto a bird’s-eye-view (BEV) plane to obtain geometry-aligned representations en-

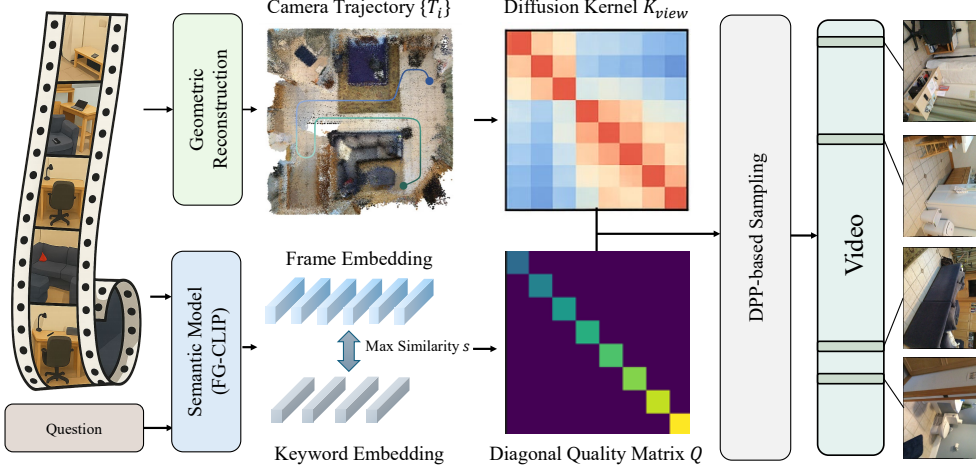


Figure 3. **Macro Perception.** Given an input video and a question, we first reconstruct the scene geometry and camera trajectory in  $SE(3)$  to build a sparse pose graph, whose heat-kernel diffusion yields the viewpoint kernel  $K_{\text{view}}$ . In parallel, FG-CLIP [35] computes frame–keyword similarities that are temperature-calibrated into semantic scores and encoded in a diagonal quality matrix  $Q$ . The resulting DPP L-ensemble  $L_{\text{dpp}} = QK_{\text{view}}Q$  is then used to greedily select  $k$  frames.

coding camera trajectories and visible regions. In parallel, a vision–language model (e.g., FG-CLIP [35]) computes the semantic relevance between each frame and the textual query. These geometric and semantic cues are fed into the **Semantic–Perspective Fusion Determinantal Point Process (SPF-DPP)**, which selects keyframes that balance viewpoint diversity and semantic importance under a fixed token budget. SPF-DPP constructs a positive semi-definite kernel combining semantic similarity and geometric coverage, and a greedy maximum a posteriori (MAP) procedure yields an initial frame set  $\mathcal{I}_0 = \{I_i\}_{i=1}^{N_0}$  that is compact, diverse, and query-relevant.

**Micro Verification.** Given the user query, the macro-selected frame set  $\mathcal{I}_0$ , and the BEV image  $I_{\text{BEV}}$ , the multimodal CoT module maintains a reasoning state  $(\mathbf{h}_t, \mathcal{I}_t)$  at step  $t$ , where  $\mathbf{h}_t$  is the latent text–image state and  $\mathcal{I}_t$  is the current evidence set. At each step, the policy either outputs a final textual answer or invokes a BEV grounding tool with a BEV-specified camera pose  $\hat{T}_t$ . The tool queries the SLAM reconstruction and retrieves the video frame whose estimated pose is closest to  $\hat{T}_t$  under a scale-aware  $SE(3)$  pose-distance metric, and the retrieved frame  $I_{t+1}$  is added to the evidence set, updating  $\mathcal{I}_{t+1} = \mathcal{I}_t \cup \{I_{t+1}\}$ . This closed-loop interaction lets the model actively acquire complementary viewpoints when evidence is insufficient, enabling adaptive, geometry-aware reasoning over the video. The multimodal CoT policy is trained with our **Zero-RL** pipeline using only spatial and answer-level rewards, without any supervised SFT on intermediate reasoning steps.

#### 4.1. SPF-DPP for macro perception

**Task Definition.** As shown in Fig. 3, given a video with  $N$  frames, each frame  $i$  has a camera pose  $T_i = (R_i, \mathbf{t}_i) \in$

$SE(3)$  and a semantic score  $s_i \in [0, 1]$  calculated w.r.t. the query. Our goal is to select a fixed-size subset  $X \subseteq \{1, \dots, N\}$  with  $|X| = k$  that is diverse in viewpoint while semantically representative.

**Pose Distance and Sparse Viewpoint Graph.** We measure geometry in  $SE(3)$  by a scale-aware distance:

$$d_{ij}^2 = \underbrace{\|\mathbf{t}_i - \mathbf{t}_j\|^2 / \sigma_t^2}_{\text{translation}} + \underbrace{\beta^2 \theta(R_i, R_j)^2}_{\text{rotation}}$$

$$\theta(R_i, R_j) = \arccos\left(\frac{\text{tr}(R_i^T R_j) - 1}{2}\right)$$

where  $\sigma_t$  normalizes the scale of the scene and  $\beta$  balances the radians against the meters. We convert distance into an affinity:

$$w_{ij} = \exp(-\frac{1}{2}d_{ij}^2).$$

and then keep edges only within a local temporal neighborhood:

$$W_{ij} = \begin{cases} w_{ij}, & \text{if } |i - j| \leq b, \\ 0, & \text{otherwise,} \end{cases}$$

yields a sparse and symmetric adjacency  $W = [W_{ij}]$  with bandwidth  $2b+1$ . This construction makes the subsequent diffusion kernel linear in the number of frames and aligns with our streaming pre-processing.

**Diffusion viewpoints kernel.** We use symmetric normalized Laplacian  $\mathcal{L} = I - D^{-1/2}WD^{-1/2}$  and define a heat-kernel diffusion:

$$K_{\text{view}} = \exp(-\tau \mathcal{L}),$$

with scale  $\tau > 0$ . This construction yields a positive semidefinite (PSD) kernel that propagates local viewpoint affinities to global relations.

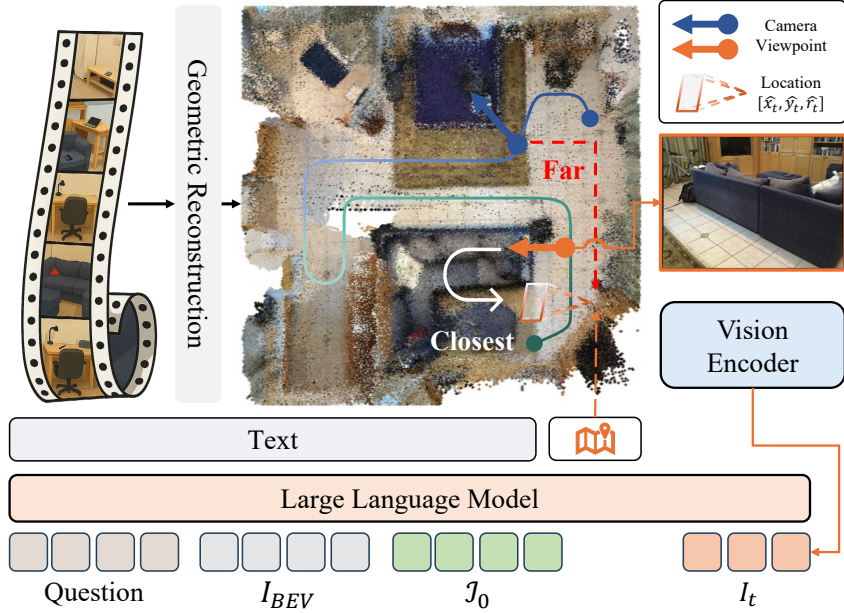


Figure 4. **Spatial MCoT for Micro Verification.** The model begins with videos, questions and BEV image, then queries on the BEV plane, retrieves the nearest video frame as an activity observation, encodes it using a visual encoder, and feeds it into a large language model to generate interleaved spatial thought chains for iterative spatial reasoning and thinking.

**Semantic Score and Quality Modulation.** Raw semantic scores  $s_i$  are calibrated to mitigate scale and tail effects:

$$\tilde{s}_i = \text{norm}_{0-1}\left(\frac{\exp(s_i/T)}{\sum_j \exp(s_j/T)}\right), \quad T > 0.$$

We define a diagonal quality matrix

$$Q = \text{diag}(q_1, \dots, q_N), q_i = (1 - \alpha) + \alpha \tilde{s}_i, \alpha \in [0, 1],$$

which biases selection toward semantically relevant frames while keeping a nonzero floor ( $1 - \alpha$ ) to preserve diversity.

**L-ensemble kernel and fixed-size MAP.** The DPP L-ensemble kernel is

$$L_{\text{dpp}} = Q K_{\text{view}} Q,$$

which is PSD because  $K_{\text{view}}$  is PSD and  $Q$  is diagonal non-negative. For a fixed budget  $k$ , we solve

$$\max_{X \subseteq [N], |X|=k} \log \det(L_{\text{dpp},X}),$$

where  $L_{\text{dpp},X}$  is the principal submatrix indexed by  $X$ . We use the standard greedy MAP with rank-one Cholesky updates; this gives a  $(1 - 1/e)$ -approximation for the equivalent monotone submodular objective under a cardinality constraint and runs in  $\mathcal{O}(kN\bar{r} + k^2N)$  time, where  $\bar{r}$  is the average number of nonzeros per row in  $K_{\text{view}}$  (dominated by the  $k$ NN sparsity and the polynomial degree  $m$ ). Furthermore, the details of the SPF-DPP with the hyperparameter are shown in supplemental material.

## 4.2. Spatial MCoT for Micro Verification

**Problem as an MDP.** The micro verification is as the multi-modal CoT in the EagleVision. Specifically, we cast EagleVision’s multi-modal CoT as a finite-horizon Markov Decision Process (MDP)  $\mathcal{M} = (\mathcal{S}, \mathcal{A}, \mathcal{T}, \mathcal{R}, \gamma)$ . In step  $t$ , the state is

$$s_t = (\mathbf{X}_{\leq t}, \mathbf{I}_{\leq t}, \mathcal{B})$$

concatenates all generated text tokens  $\mathbf{X}_{\leq t}$ , all retrieved visual observations  $\mathbf{I}_{\leq t}$ , and a BEV camera pose location buffer  $\mathcal{B}$ . The action space is *interleaved*:

$$\mathcal{A} = \{\text{TOKEN}(y)\} \cup \{\text{QUERY}(\hat{p})\} \cup \{\text{STOP}\},$$

where  $\text{TOKEN}(y)$  emits the next text token  $y$ ,  $\text{QUERY}(\hat{p})$  issues a pose query on the BEV plane, and  $\text{STOP}$  terminates with the current answer.

**BEV-grounded Agent.** In each reasoning step, the agent predicts a 2D BEV pose  $\hat{p}_t = (\hat{x}_t, \hat{y}_t, \hat{r}_t)$ , where  $(\hat{x}_t, \hat{y}_t)$  denotes the BEV coordinates and  $\hat{r}_t$  is the angle of orientation in the plane ( $r=0$  corresponds to the direction  $(x=0, y=-1)$ , increasing clockwise).

For each video frame  $j$ , we store its BEV-projected position  $(x_j, y_j)$  and orientation  $r_j$  obtained during preprocessing. The spatial similarity between the queried pose and each frame is defined directly on the BEV plane as follows.

$$s_{tj} = \exp\left[-\frac{1}{2}(\|(\hat{x}_t, \hat{y}_t) - (x_j, y_j)\|^2/\sigma_p^2 + \beta^2(\hat{r}_t - r_j)^2)\right],$$

where  $\sigma_p$  controls the spatial scale and  $\beta$  balances rotation

Methods	Rank	Avg.	Obj. Count	Abs. Dist.	Obj. Size	Room Size	Rel. Dist.	Rel. Dir.	Route Plan	Appr. Order	Numerical Answer		Multiple-Choice Answer	
											Numerical Answer		Multiple-Choice Answer	
<i>Baseline</i>														
Chance Level (Random)	-	-	-	-	-	-	25.0	36.1	28.3	25.0				
Chance Level (Frequency)	-	34.0	62.1	32.0	29.9	33.1	25.1	47.9	28.4	25.2				
<i>VSI-Bench Perf. (<math>\dagger</math>= Tiny Set)</i>													[38]	
$\dagger$ Human Level	-	79.2	94.3	47.0	60.4	45.9	94.7	95.8	95.8	100.0				
$\dagger$ Gemini-1.5 Flash [2]	-	45.7	50.8	33.6	56.5	45.2	48.0	39.8	32.7	59.2				
$\dagger$ Gemini-1.5 Pro [2]	-	48.8	49.6	28.8	58.6	49.4	46.0	48.1	42.0	68.0				
$\dagger$ Gemini-2.0 Flash [2]	-	45.4	52.4	30.6	66.7	31.8	56.0	46.3	24.5	55.1				
<i>Proprietary Models (API)</i>														
GPT-4o [19]	3	34.0	46.2	5.3	43.8	38.2	37.0	41.3	31.5	28.5				
Gemini-1.5 Flash [2]	2	42.1	49.8	30.8	53.5	54.4	37.7	41.0	31.5	37.8				
Gemini-1.5 Pro [2]	1	45.4	56.2	30.9	64.1	43.6	51.3	46.3	36.0	34.6				
<i>Open-sourced VLMs</i>														
InternVL2-2B [7]	14	27.4	21.8	24.9	22.0	35.0	33.8	44.2	30.5	7.1				
LLaVA-OneVision-0.5B [21]	13	28.0	46.1	28.4	15.4	28.3	28.9	36.9	34.5	5.8				
LongVA-7B [43]	12	29.2	38.0	16.6	38.9	22.2	33.1	43.3	25.4	15.7				
LLaVA-OneVision-7B [21]	11	32.4	47.7	20.2	47.4	12.3	42.5	35.2	29.4	24.4				
InternVL2-8B [7]	10	34.6	23.1	28.7	48.2	39.8	36.7	30.7	29.9	39.6				
LLaVA-NeXT-Video-7B [20]	9	35.6	48.5	14.0	47.8	24.2	43.5	42.4	34.0	30.6				
Qwen2.5-VL-7B [3]	8	35.8	-	-	-	-	-	-	-	-				
InternVL2-40B [7]	7	36.0	34.9	26.9	46.5	31.8	42.1	32.2	34.0	39.6				
LLaVA-NeXT-Video-72B [20]	6	40.9	48.9	22.8	57.4	35.3	42.4	36.7	35.0	48.6				
LLaVA-OneVision-72B [21]	5	40.2	43.5	23.9	57.6	37.5	42.5	39.9	32.5	44.6				
SpaceR-7B [25]	4	44.5	-	-	-	-	-	-	-	-				
VILASR-7B [34]	3	45.4	-	-	-	-	-	-	-	-				
Qwen3-VL-8B [37]	3	59.4	-	-	-	-	-	-	-	-				
VLM-3R-7B [12]	2	60.9	70.2	49.4	69.2	67.1	65.4	80.5	45.4	40.1				
<b>EagleVision (Ours)</b>	<b>1</b>	<b>63.5</b>	<b>74.9</b>	<b>41.3</b>	<b>72.3</b>	<b>69.4</b>	<b>70.1</b>	<b>84.7</b>	<b>46.3</b>	<b>49.3</b>				

Table 1. **Evaluations on VSI-Bench.** Eaglevision ranks first among open-sourced VLMs, showcasing the effectiveness of our dual stage framework.  $\dagger$ Results on the VSI-Bench tiny set are presented following the setup in [38].

sensitivity. The frame with the highest similarity

$$j^* = \arg \max_j s_{tj}, \quad s_{\max}^{(t)} = s_{tj^*},$$

Returns when  $s_{\max}^{(t)} \geq \tau_s$ ; otherwise, the agent outputs an error prompt. The frame retrieved  $I_{j^*}$  is attached to the observation set  $I_{\leq t}$ , and the number of agent calls is capped by  $T_{\max}$ .

**Reward Function.** The overall trajectory reward consists of answer-level and spatial terms:

$$R(\tau) = R_{\text{acc}}(\tau) + R_{\text{format}}(\tau) + \lambda_{\text{tool}} R_{\text{tool}}(\tau) + \lambda_{\text{spatial}} R_{\text{spatial}}(\tau)$$

We define a spatial reward to penalize trajectories that rely on low-quality spatial grounding. Let  $\mathcal{C}(\tau) \subseteq \{1, \dots, T\}$  denote the set of time steps at which the spatial tool based on BEV is invoked along the trajectory  $\tau$ . For each call  $t \in \mathcal{C}(\tau)$ , let  $s_{\max}^{(t)} = \max_k s(q^{(t)}, f_k^{(t)})$  be the maximum similarity score between the query representation  $q^{(t)}$  and the frame candidates retrieved  $\{f_k^{(t)}\}$  under a similarity function  $s(\cdot, \cdot)$ . We then compare  $s_{\max}^{(t)}$  to a fixed

similarity threshold  $\theta_{\text{sim}} > 0$  and assign a trajectory-level spatial penalty:

$$R_{\text{spatial}}(\tau) = \begin{cases} -\alpha_s, & \text{if } \exists t \in \mathcal{C}(\tau) \text{ s.t. } s_{\max}^{(t)} < \theta_{\text{sim}}, \\ 0, & \text{otherwise,} \end{cases}$$

where  $\alpha_s > 0$  controls the magnitude of the penalty. In other words, calling the spatial tool  $N$  times but having low-similarity retrievals yields the same penalty  $-\alpha_s$ , which encourages the model to maintain accurate BEV grounding instead of repeatedly probing regions that lack reliable camera coverage.

**Optimization.** We train the agent using Group Relative Policy Optimization (GRPO) [14], which estimates the advantages within the prompt-level trajectory groups to reduce variance. A frozen reference policy provides KL regularization for stability. During training, the VLM policy  $\pi_\theta$  generates actions in an interleaved manner until the STOP or Step limit is reached. Only model-generated text tokens are included in the reward computation, while retrieved observations and tool metadata are masked out.

MCOT	BEV	SPF-DPP	Avg.
	Baseline (Qwen3-VL-8B)		59.4
✓			61.9
✓	✓		62.7
✓		✓	62.5
✓	✓	✓	63.5

Table 2. Ablation study about structure of EagleVision.

## 5. Experiment

### 5.1. Implement Details

**Baselines and Benchmarks.** We compared our model with four baseline categories: (1) randomized heuristics (random and frequency-based choices), (2) proprietary large-scale models (e.g. *Gemini-1.5* [2], *Gemini-2.0* [2]), (3) open-source vision-language models (e.g. *Qwen3-VL-8B* [37], *LLaVA-OneVision-72B* [21]), and (4) task-specific methods (e.g. *VLM-3R-7B* [12]) tailored for spatial reasoning. Evaluations were conducted on VSI-Bench [38], which assesses 3D spatial understanding in video-language models in configuration and measurement tasks. All models were tested with identical video input and question templates to ensure fair comparison.

**Training Details.** We finetune Qwen3-VL-8B [37] by implementing GRPO [14] across 80 cycles using H20 GPUs. Each batch comprises 256 chosen prompts, with 16 rollouts per prompt and a limit of six tool call steps. The KL coefficient is kept at 0.0, and the response length is restricted to 20,480 tokens.

### 5.2. Evaluations

**VSI-Bench.** As depicted in Tab. 1, EagleVision exhibits highly competitive results on the VSI-Bench benchmark [38], effectively boosting the spatial intelligence of large language models (LLMs) without modifying the model’s input. By integrating the thinking-with-space (TWS) mechanism, EagleVision consistently and significantly enhances outcomes across all tasks, especially in sequence reasoning. Compared to the baseline Qwen3-VL-8B [37], our model shows an overall improvement of 4.1 points, underscoring the effectiveness of DPP sampling and the TWS reasoning chain. In contrast to VLM-3R-7B [12], EagleVision achieves a 3.6-point enhancement without reconstructing or augmenting spatial input. Despite a noticeable gap from human-level performance, EagleVision exceeds human accuracy in fine-grained spatial distance estimation, showcasing its strong potential for cognition tasks.

### 5.3. Ablation Study

We conduct ablation studies to assess the effectiveness and contribution of our proposed multi-modal data and the model components. All variants of the ablated model are

w/o DPP	Geometry	Semantic	Avg.
✓			62.7
	✓		63.2
		✓	63.0
	✓	✓	63.5

Table 3. Ablation study about SPF-DPP.

Acc.	Format	Tool	Spatial	Avg.
✓	✓			61.1
✓	✓	✓		63.0
✓	✓	✓	✓	63.5

Table 4. Ablation study about Reward function. Acc. means the accuracy reward.

trained using the VLM-3R dataset [12]. Evaluations are performed in VSI-Bench [38] following the identical experimental setup used for EagleVision. More ablation studies are shown in supplemental material.

**Overall Architecture.** We ablate the three key components of EagleVision: MCoT, BEV grounding, and SPF-DPP on Qwen3-VL-8B (59.4 Avg), as shown in Tab. 2. Adding MCoT alone improves to 61.9, showing that iterative multimodal reasoning enhances spatial awareness. Introducing BEV grounding further lifts performance to 62.7, confirming the benefit of explicit geometric anchoring. Replacing BEV with SPF-DPP yields 62.5, indicating that balanced, query-aware frame sampling strengthens evidence quality. Combining all three achieves the best 63.5, demonstrating their complementarity: MCoT structures reasoning, BEV enforces spatial consistency, and SPF-DPP optimizes visual evidence.

**SPF-DPP.** Tab. 3 ablates the two SPF-DPP components, geometry-aware diffusion and semantic modulation, on the MCoT+BEV baseline (62.7). Enabling Geometry alone reaches 63.2 (+0.5), improving viewpoint diversity via pose-aware similarity. Enabling Semantic alone gives 63.0 (+0.3), favoring task-relevant frames. Using both achieves 63.5 (+0.8), indicating that geometry enhances spatial coverage while semantics biases selection toward informative evidence.

**GRPO Reward Ablation.** We further ablate GRPO reward terms: Accuracy (Acc), Format, Tool bonus, and Spatial consistency in Tab. A6. Acc+Format yields 61.1. Adding Tool boosts performance to 63.0 (+1.9), showing that outcome-conditioned encouragement of tool use is crucial. Adding the Spatial term reaches 63.5 (+0.5), by rewarding pose-consistent calls and penalizing invalid retrievals. Overall, the Tool reward provides the main gain, while Spatial further regularizes decisions for stable improvements.

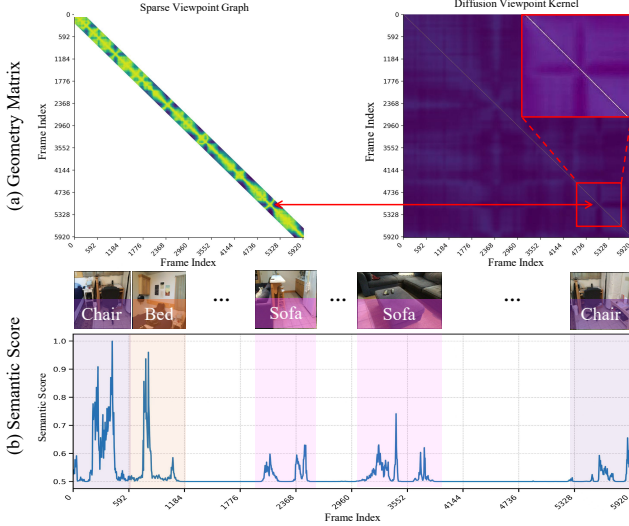


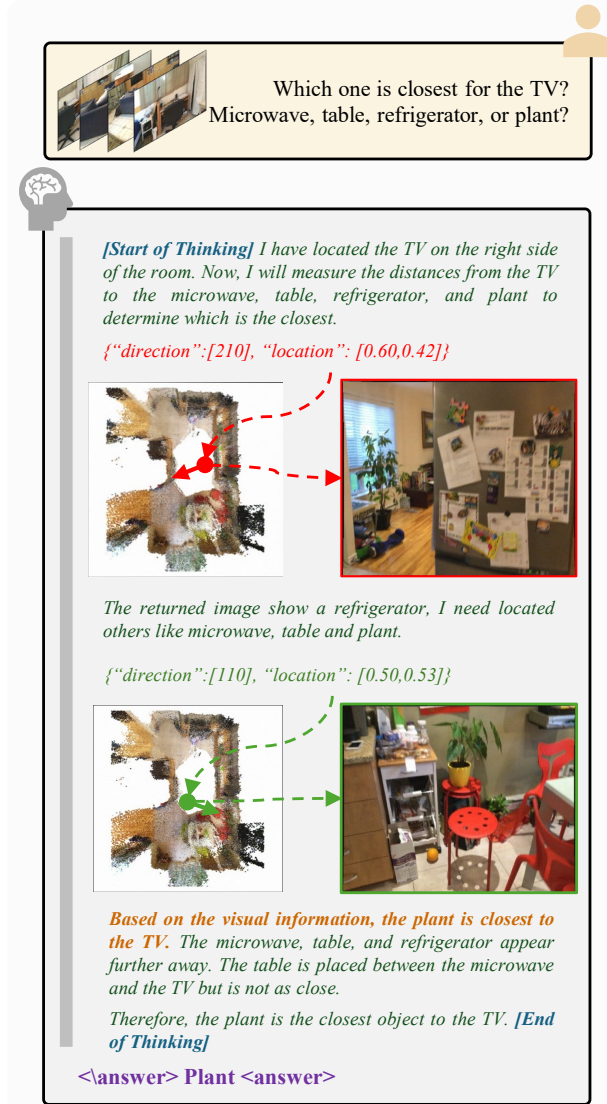
Figure 5. Visualization of SPF-DPP of Scannet Scene00\_00. (a) The matrix of Sparse Viewpoint Graph and Diffusion Viewpoint Kernel. The smaller sub-figure serves as an enhancement. (b) The Semantic Score and related video frame. The keyword of question is chair, bed and sofa, as similar as the Fig. 1.

#### 5.4. Visualization

**Sparse Viewpoint Graph and Diffusion Viewpoint Kernel.** Fig. 5 (a) illustrates the Sparse Viewpoint Graph alongside the Diffusion Viewpoint Kernel for Scene00\_00. In the Sparse Graph, the limited bandwidth causes numerous zero entries (white areas), and the similarity  $W_{ij}$  tends to diminish as the temporal gap widens, although this rate of decrease varies over time. When comparing the Sparse Graph to the diffusion kernel, it is evident that rapid camera movements result in more pronounced off-diagonal attenuation in the diffusion kernel. This demonstrates its sensitivity to changes in viewpoint and its capacity to maintain local consistency. Significant pose shifts intensify high-frequency Laplacian components, making the diffusion kernel rapidly decrease in non-local areas. This behavior adaptively reduces similarities across substantial viewpoint changes while preserving locally coherent structures.

**Semantic Score.** Fig. 5 (b) shows the semantic scores of each video frame for the keywords *chair*, *bed*, and *sofa*, along with representative frames at peak scores. The semantic scores accurately localize frames relevant to each keyword but remain sparse over the full sequence. Thus, only by jointly leveraging semantic and geometric cues can we ensure both task relevance and spatial consistency.

**Model Response.** As depicted in Fig. 6, the model’s response example is presented. Upon receiving the video input, the model employs a secondary localization process on each object in sequence to ascertain their proximity to the TV. Initially, the model localizes the refrigerator, followed by secondary localization of the table and the plant. After conducting localization and analysis, the model determines



that the plant is the nearest object. Consequently, the analysis confirms the plant as the closest object to the TV.

#### 6. Conclusion

We present EagleVision, a dual-phase framework for multimodal spatial reasoning through macro perception and micro verification. For macro perception, we propose SPF-DPP, jointly optimizing semantic importance and view diversity for geometry-aware frame selection under a token budget. For micro verification, we operationalize spatial CoT through BEV-based pose querying and train the querying policy by pure reinforcement learning with spatial reward, without CoT supervision. In future work, our aim is to reduce the dependency on external models and pursue a more unified, end-to-end architecture for efficient spatial reasoning.

## References

[1] Hervé Abdi and Lynne J Williams. Principal component analysis. *Wiley interdisciplinary reviews: computational statistics*, 2(4):433–459, 2010. 1

[2] Rohan Anil, Sebastian Borgeaud, Ethan Dyer, and et al. Gemini 1.5: Unlocking multimodal understanding across millions of tokens of context. *arXiv preprint arXiv:2403.05530*, 2024. 6, 7

[3] Jinze Bai, Shuai Bai, Shusheng Yang, Shijie Wang, Sinan Tan, Peng Wang, Junyang Lin, Chang Zhou, and Jingren Zhou. Qwen-vl: A frontier large vision-language model with versatile abilities. *arXiv preprint arXiv:2308.12966*, 2023. 2, 6

[4] Xiao Bai, Pengcheng Zhang, Xiaohan Yu, Jin Zheng, Edwin R Hancock, Jun Zhou, and Lin Gu. Learning from human attention for attribute-assisted visual recognition. *IEEE Transactions on Pattern Analysis and Machine Intelligence*, 2024. 2

[5] CK Chan and ST Tan. Determination of the minimum bounding box of an arbitrary solid: an iterative approach. *Computers & Structures*, 79(15):1433–1449, 2001. 1

[6] Boyuan Chen, Zhuo Xu, Sean Kirmani, Brain Ichter, Dorsa Sadigh, Leonidas Guibas, and Fei Xia. Spatialvlm: Endowing vision-language models with spatial reasoning capabilities. In *CVPR*, pages 14455–14465, 2024. 1, 2

[7] Zhe Chen, Jiannan Wu, Wenhui Wang, Weijie Su, Guo Chen, Sen Xing, Muyan Zhong, Qinglong Zhang, Xizhou Zhu, Lewei Lu, et al. Internvl: Scaling up vision foundation models and aligning for generic visual-linguistic tasks. In *CVPR*, 2024. 6

[8] An-Chieh Cheng, Hongxu Yin, Yang Fu, Qiushan Guo, Ruihan Yang, Jan Kautz, Xiaolong Wang, and Sifei Liu. Spatial-rpt: Grounded spatial reasoning in vision language models. *arXiv preprint arXiv:2406.01584*, 2024. 1, 2

[9] Jiajun Deng, Tianyu He, Li Jiang, Tianyu Wang, Feras Dayoub, and Ian Reid. 3d-llava: Towards generalist 3d llms with omni superpoint transformer. *arXiv*, 2025. 2

[10] Yuhao Dong, Zuyan Liu, Hai-Long Sun, Jingkang Yang, Winston Hu, Yongming Rao, and Ziwei Liu. Insight-v: Exploring long-chain visual reasoning with multimodal large language models. In *Proceedings of the Computer Vision and Pattern Recognition Conference*, pages 9062–9072, 2025. 2

[11] Danny Driess, Fei Xia, Mehdi SM Sajjadi, Corey Lynch, Aakanksha Chowdhery, Ayzaan Wahid, Jonathan Tompson, Quan Vuong, Tianhe Yu, Wenlong Huang, et al. Palm-e: An embodied multimodal language model. *arxiv*, 2023. 1

[12] Zhiwen Fan, Jian Zhang, Renjie Li, Junge Zhang, Runjin Chen, Hezhen Hu, Kevin Wang, Huaizhi Qu, Dilin Wang, Zhicheng Yan, et al. Vlm-3r: Vision-language models augmented with instruction-aligned 3d reconstruction. *arXiv preprint arXiv:2505.20279*, 2025. 2, 6, 7

[13] Jun Gao, Yongqi Li, Ziqiang Cao, and Wenjie Li. Interleaved-modal chain-of-thought. In *Proceedings of the Computer Vision and Pattern Recognition Conference*, pages 19520–19529, 2025. 2

[14] Daya Guo, Dejian Yang, Haowei Zhang, Junxiao Song, Peiyi Wang, Qihao Zhu, Runxin Xu, Ruoyu Zhang, Shirong Ma, Xiao Bi, et al. Deepseek-r1 incentivizes reasoning in llms through reinforcement learning. *Nature*, 645(8081):633–638, 2025. 6, 7

[15] Xiaoshuai Hao, Ruikai Li, Hui Zhang, Dingzhe Li, Rong Yin, Sangil Jung, Seung-In Park, ByungIn Yoo, Haimei Zhao, and Jing Zhang. Mapdistill: Boosting efficient camera-based hd map construction via camera-lidar fusion model distillation. In *European Conference on Computer Vision*, pages 166–183. Springer, 2024. 1

[16] Jack Hong, Chenxiao Zhao, ChengLin Zhu, Weiheng Lu, Guohai Xu, and Xing Yu. Deepeyesv2: Toward agentic multimodal model. *arXiv preprint arXiv:2511.05271*, 2025. 2

[17] Yining Hong, Haoyu Zhen, Peihao Chen, Shuhong Zheng, Yilun Du, Zhenfang Chen, and Chuang Gan. 3d-llm: Injecting the 3d world into large language models. In *NeurIPS*, 2023. 2

[18] Jiahui Huang, Qunjie Zhou, Hesam Rabeti, Aleksandr Kordova, Huan Ling, Xuanchi Ren, Tianchang Shen, Jun Gao, Dmitry Slepichev, Chen-Hsuan Lin, et al. Vipe: Video pose engine for 3d geometric perception. *arXiv preprint arXiv:2508.10934*, 2025. 3, 1

[19] Aaron Hurst, Adam Lerer, Adam P Goucher, Adam Perelman, Aditya Ramesh, Aidan Clark, AJ Ostrow, Akila Welihinda, Alan Hayes, Alec Radford, et al. Gpt-4o system card. *arXiv*, 2024. 2, 6

[20] Bo Li, Kaichen Zhang, Hao Zhang, Dong Guo, Renrui Zhang, Feng Li, Yuanhan Zhang, Ziwei Liu, and Chunyuan Li. Llava-next: Stronger llms supercharge multimodal capabilities in the wild, 2024. 6

[21] Bo Li, Yuanhan Zhang, Dong Guo, Renrui Zhang, Feng Li, Hao Zhang, Kaichen Zhang, Peiyuan Zhang, Yanwei Li, Ziwei Liu, et al. Llava-onevision: Easy visual task transfer. *arXiv*, 2024. 6, 7

[22] Yunze Man, Liang-Yan Gui, and Yu-Xiong Wang. Situational awareness matters in 3d vision language reasoning. In *Proceedings of the IEEE/CVF Conference on Computer Vision and Pattern Recognition*, pages 13678–13688, 2024. 2

[23] OpenAI. Thinking with images. <https://openai.com/index/thinking-with-images/>, 2025. 2

[24] Joseph O’Rourke. Finding minimal enclosing boxes. *International journal of computer & information sciences*, 14(3):183–199, 1985. 1

[25] Kun Ouyang, Yuanxin Liu, Haoning Wu, Yi Liu, Hao Zhou, Jie Zhou, Fandong Meng, and Xu Sun. Spacer: Reinforcing mllms in video spatial reasoning. *arXiv preprint arXiv:2504.01805*, 2025. 6

[26] Zekun Qi, Runpei Dong, Shaochen Zhang, Haoran Geng, Chunrui Han, Zheng Ge, Li Yi, and Kaisheng Ma. Shapellm: Universal 3d object understanding for embodied interaction. In *European Conference on Computer Vision*, pages 214–238. Springer, 2024. 2

[27] Manish Sanwal. Layered chain-of-thought prompting for multi-agent llm systems: A comprehensive approach to explainable large language models. *arXiv preprint arXiv:2501.18645*, 2025. 2

[28] Manolis Savva, Abhishek Kadian, Oleksandr Maksymets, Yili Zhao, Erik Wijmans, Bhavana Jain, Julian Straub, Jia

Liu, Vladlen Koltun, Jitendra Malik, et al. Habitat: A platform for embodied ai research. In *Proceedings of the IEEE/CVF international conference on computer vision*, pages 9339–9347, 2019. 2

[29] Hao Shan, Ruihai Li, Han Jiang, Yizhe Fan, Ziyang Yan, Bohan Li, Xiaoshuai Hao, Hao Zhao, Zhiyong Cui, Yilong Ren, et al. Stability under scrutiny: Benchmarking representation paradigms for online hd mapping. *arXiv preprint arXiv:2510.10660*, 2025. 1

[30] Jiaxu Wan, Hong Zhang, Ziqi He, Yangyan Deng, Qishu Wang, Ding Yuan, and Yifan Yang. Sp2t: Sparse proxy attention for dual-stream point transformer. In *Proceedings of the IEEE/CVF International Conference on Computer Vision*, pages 27885–27895, 2025. 2

[31] Haochen Wang, Yucheng Zhao, Tiancai Wang, Haoqiang Fan, Xiangyu Zhang, and Zhaoxiang Zhang. Ross3d: Reconstructione visual instruction tuning with 3d-awareness. *arXiv preprint arXiv:2504.01901*, 2025. 2

[32] Jianyuan Wang, Minghao Chen, Nikita Karaev, Andrea Vedaldi, Christian Rupprecht, and David Novotny. Vggt: Visual geometry grounded transformer. *arXiv preprint arXiv:2503.11651*, 2025. 1

[33] Shuzhe Wang, Vincent Leroy, Yohann Cabon, Boris Chidlovskii, and Jerome Revaud. Dust3r: Geometric 3d vision made easy. In *Proceedings of the IEEE/CVF Conference on Computer Vision and Pattern Recognition*, pages 20697–20709, 2024. 1, 2

[34] Junfei Wu, Jian Guan, Kaituo Feng, Qiang Liu, Shu Wu, Liang Wang, Wei Wu, and Tieniu Tan. Reinforcing spatial reasoning in vision-language models with interwoven thinking and visual drawing. *arXiv preprint arXiv:2506.09965*, 2025. 1, 6

[35] Chunyu Xie, Bin Wang, Fanjing Kong, Jincheng Li, Dawei Liang, Gengshen Zhang, Dawei Leng, and Yuhui Yin. Fg-clip: Fine-grained visual and textual alignment. *arXiv preprint arXiv:2505.05071*, 2025. 4

[36] Mengwei Xie, Shuang Zeng, Xinyuan Chang, Xinran Liu, Zheng Pan, Mu Xu, and Xing Wei. Seqgrowgraph: Learning lane topology as a chain of graph expansions. In *Proceedings of the IEEE/CVF International Conference on Computer Vision (ICCV)*, pages 27166–27175, 2025. 1

[37] An Yang, Anfeng Li, Baosong Yang, Beichen Zhang, Binyuan Hui, Bo Zheng, Bowen Yu, Chang Gao, Chen-gen Huang, Chenxu Lv, Chujie Zheng, Dayiheng Liu, Fan Zhou, Fei Huang, Feng Hu, Hao Ge, Haoran Wei, Huan Lin, Jialong Tang, Jian Yang, Jianhong Tu, Jianwei Zhang, Jianxin Yang, Jiaxi Yang, Jing Zhou, Jingren Zhou, Junyang Lin, Kai Dang, Keqin Bao, Kexin Yang, Le Yu, Lianghao Deng, Mei Li, Mingfeng Xue, Mingze Li, Pei Zhang, Peng Wang, Qin Zhu, Rui Men, Ruize Gao, Shixuan Liu, Shuang Luo, Tianhao Li, Tianyi Tang, Wenbiao Yin, Xingzhang Ren, Xinyu Wang, Xinyu Zhang, Xuancheng Ren, Yang Fan, Yang Su, Yichang Zhang, Yinger Zhang, Yu Wan, Yuqiong Liu, Zekun Wang, Zeyu Cui, Zhenru Zhang, Zhipeng Zhou, and Zihan Qiu. Qwen3 technical report. *arXiv preprint arXiv:2505.09388*, 2025. 6, 7

[38] Jihan Yang, Shusheng Yang, Anjali W Gupta, Rilyn Han, Li Fei-Fei, and Saining Xie. Thinking in space: How multimodal large language models see, remember, and recall spaces. *arXiv*, 2024. 2, 6, 7

[39] Beibei Yu, Tao Shen, and Ling Chen. Sta-cot: Structured target-centric agentic chain-of-thought for consistent multi-image geological reasoning. In *Findings of the Association for Computational Linguistics: EMNLP 2025*, pages 25426–25444, 2025. 2

[40] Hong Zhang, Jiaxu Wan, Ziqi He, Jianbo Song, Yifan Yang, and Ding Yuan. Sparse agent transformer for unified voxel and image feature extraction and fusion. *Information Fusion*, 110:102455, 2024. 2

[41] Hong Zhang, Jiaxu Wan, Jing Zhang, Ding Yuan, Xuliang Li, and Yifan Yang. P2ftrack: Multi-object tracking with motion prior and feature posterior. *ACM Transactions on Multimedia Computing, Communications and Applications*, 21(1):1–22, 2024. 1

[42] Jiawei Zhang, Lei Huang, Xiao Bai, Jin Zheng, Lin Gu, and Edwin Hancock. Exploring the usage of pre-trained features for stereo matching. *International Journal of Computer Vision*, 132(10):4305–4326, 2024. 1

[43] Peiyuan Zhang, Kaichen Zhang, Bo Li, Guangtao Zeng, Jingkang Yang, Yuanhan Zhang, Ziyue Wang, Haoran Tan, Chunyuan Li, and Ziwei Liu. Long context transfer from language to vision. *arXiv*, 2024. 6

[44] Pengcheng Zhang, Xiaohan Yu, Xiao Bai, Jin Zheng, Xin Ning, and Edwin R Hancock. Fully decoupled end-to-end person search: An approach without conflicting objectives. *International Journal of Computer Vision*, pages 1–22, 2025. 2

[45] Qingqing Zhao, Yao Lu, Moo Jin Kim, Zipeng Fu, Zhuoyang Zhang, Yecheng Wu, Zhaoshuo Li, Qianli Ma, Song Han, Chelsea Finn, et al. Cot-vla: Visual chain-of-thought reasoning for vision-language-action models. In *Proceedings of the Computer Vision and Pattern Recognition Conference*, pages 1702–1713, 2025. 2

[46] Duo Zheng, Shijia Huang, and Liwei Wang. Video-3d llm: Learning position-aware video representation for 3d scene understanding. *arXiv*, 2024. 2

[47] Ziwei Zheng, Michael Yang, Jack Hong, Chenxiao Zhao, Guohai Xu, Le Yang, Chao Shen, and Xing Yu. Deep-eyes: Incentivizing “thinking with images” via reinforcement learning. *arXiv preprint arXiv:2505.14362*, 2025. 2

[48] Chenming Zhu, Tai Wang, Wenwei Zhang, Jiangmiao Pang, and Xihui Liu. Llava-3d: A simple yet effective pathway to empowering llmms with 3d-awareness. *arXiv*, 2024. 2

# EagleVision: A Dual-Stage Framework with BEV-grounding-based Chain-of-Thought for Spatial Intelligence

## Supplementary Material

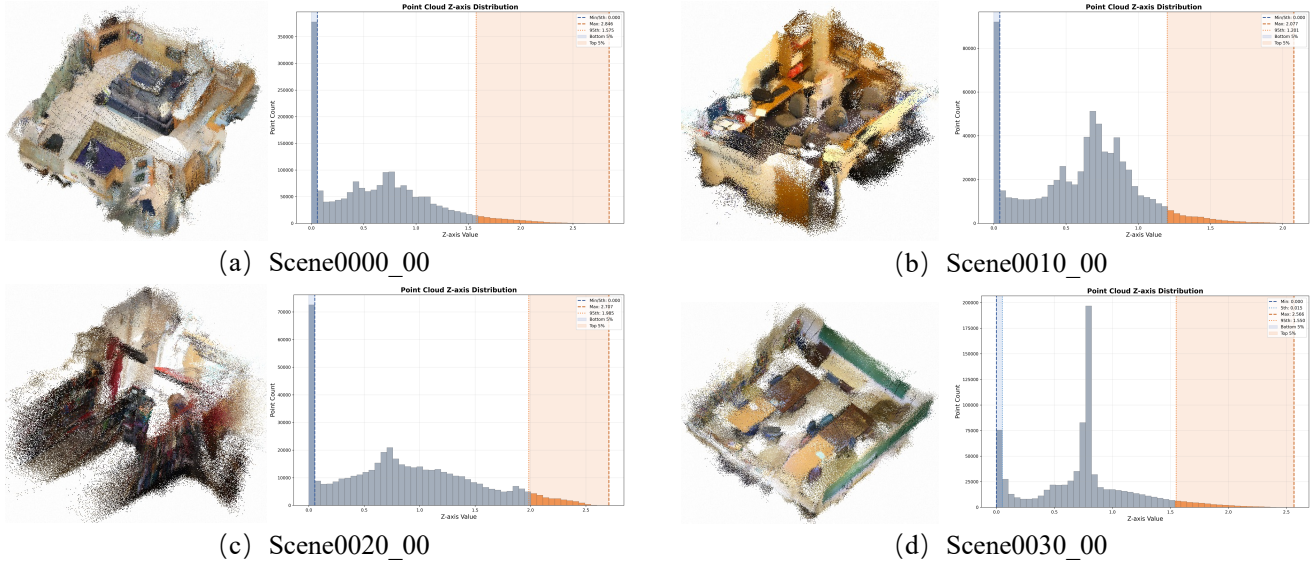


Figure A7. Visualization of point cloud and z-axis histogram.

## A. 3D Reconstruction Pre-processing Pipeline

We build a lightweight 3D reconstruction pre-processing pipeline that converts raw videos into a ground-aligned bird's-eye-view (BEV) representation. It consists of four steps: multi-view 3D reconstruction, point cloud bounding-box normalization, ground-aware plane estimation, and BEV generation.

### A.1. Multi-view 3D Reconstruction

Given an input video sequence  $\{I_t\}$ , we reconstruct the scene using vipe [18], which estimates extrinsics of the camera per-frame ( $R_t, \mathbf{t}_t$ ) and a dense depth map  $D_t$ . With camera intrinsics  $K$ , each pixel  $\mathbf{u} = (u, v)$  in frame  $t$  with depth  $D_t(\mathbf{u})$  is back-projected as

$$\mathbf{X}_t(\mathbf{u}) = R_t^{-1}(D_t(\mathbf{u})K^{-1}\tilde{\mathbf{u}} - \mathbf{t}_t), \quad (1)$$

where  $\tilde{\mathbf{u}}$  is the homogeneous coordinate of  $\mathbf{u}$ . Aggregating points from all frames produces a scene-level point cloud  $\mathcal{P}$  in a global coordinate system.

### A.2. Point Cloud Bounding-box Normalization

We estimate the Oriented Bounding Box (OBB) of  $\mathcal{P}$  and obtain its three dimensions with side lengths  $l_x, l_y, l_z$ . While PCA-based methods [1] are computationally efficient, they often fail to produce tight bounding boxes as they

are driven by data variance rather than geometric bounds. Conversely, exact algorithms based on the rotating calipers paradigm [24] guarantee minimal volume but suffer from cubic complexity ( $O(n^3)$ ), rendering them impractical for large-scale point clouds. To address this, we adopt an optimization-based approximation strategy [5]. Specifically, we formulate the orientation estimation as an optimization problem to iteratively refine the bounding box, achieving a balance between computational efficiency and volume minimization.

Upon determining the OBB, we identify the plane defined by the two largest dimensions (assumed to be  $l_x$  and  $l_y$ ) as the *candidate* scene plane  $XY$ . This is based on the empirical observation that in our target scenarios (indoor and driving scenes), the environment layout is generally regular, and the ground (along with the ceiling) typically spans the largest visible area. The remaining axis is assigned as the candidate vertical axis  $Z$ , noting that its direction (up vs. down) remains ambiguous at this stage.

### A.3. Ground-aware Plane Estimation

To resolve the  $Z$ -axis orientation, we exploit a simple ground prior: videos are captured near the ground, so the point cloud contains many ground points but few ceiling points. Consequently, as shown in Fig. A7, along the ver-

tical direction the distribution of points tends to exhibit a dense cluster near the ground and a long tail towards the ceiling.

Let  $\{z_i\}$  be the coordinates of all points in  $\mathcal{P}$  projected onto the candidate  $Z$  axis, and let  $z^{(0)}, z^{(5)}, z^{(95)}, z^{(100)}$  denote the empirical 0-th, 5-th, 95-th and 100-th percentiles of  $\{z_i\}$ , respectively. We then measure the spans of the lowest and highest 5% segments along the candidate  $Z$  axis:

$$d_{\text{bottom}} = z^{(5)} - z^{(0)}, \quad d_{\text{top}} = z^{(100)} - z^{(95)}. \quad (2)$$

Due to the long-tail behavior towards the ceiling, the ground side typically forms a much tighter cluster, and we empirically observe  $d_{\text{bottom}} \ll d_{\text{top}}$  in most cases. We therefore identify the side with the smaller 5% span (i.e.,  $\min(d_{\text{bottom}}, d_{\text{top}})$ ) as the ground side and fix the orientation of the  $Z$  axis accordingly. This yields a ground-aligned 3D coordinate system in which the  $XY$  plane is parallel to the estimated ground.

#### A.4. BEV Representation Generation

With the ground-aligned coordinates, we project all points in  $\mathcal{P}$  onto the  $XY$  plane and rasterize the plane into a regular grid. For each cell, we aggregate the points inside and encode simple geometric statistics (e.g., occupancy or height). This yields a BEV feature map with a consistent metric scale and orientation, which we use as a geometric prior for the downstream network.

## B. Hyper-parameter settings of SPF-DPP

SPF-DPP introduces a small set of hyper-parameters controlling geometry, diffusion, and semantic modulation. We fix all hyper-parameters across all experiments and do not tune them per dataset. The translation scale is set to  $\sigma_t = 1$ , and we weight rotational differences more strongly with  $\beta = 2$ . The temporal bandwidth is set to  $b = 24$ , corresponding to roughly one second for videos recorded at 24 FPS, which yields a sparse yet locally connected viewpoint graph. For the diffusion kernel, we use a heat scale of  $\tau = 2$ ; since the resulting matrices are moderate in size, we compute  $\exp(-\tau\mathcal{L})$  directly without polynomial approximation. For semantic calibration, we adopt a temperature  $T = 1$  and set the mixing weight of the quality to  $\alpha = 0.5$ , balancing semantic relevance and diversity. We select a fixed subset size of  $k = 32$  frames, following the setting used in prior work for fair comparison. All hyper-parameters are summarized in Table A5.

## C. Ablation Study

### C.1. Hyper-parameter of SPF-DPP

To investigate the impact of individual hyper-parameters in SPF-DPP, we conducted a component-wise ablation study

Symbol	Description	Value
$\sigma_t$	Translation scale (meters normalization)	1
$\beta$	Rotation weight (rad vs. meters)	2
$b$	Temporal bandwidth (frames)	24
$\tau$	Heat diffusion scale	2
$T$	Softmax temperature for semantic scores	1
$\alpha$	Quality mixing weight	0.5
$k$	Selected subset size (frames)	32

Table A5. Hyper-parameters used in SPF-DPP. All values are fixed across experiments.

No.	$\beta$	$\tau$	$\alpha$	$b$	Score
1	1	2.0	0.5	24	62.8
2	2	2.0	0.5	24	63.5
3	4	2.0	0.5	24	63.1
4	2	1.0	0.5	24	62.1
5	2	1.5	0.5	24	62.9
6	2	2.0	0.5	24	63.5
7	2	2.0	0.3	24	62.9
8	2	2.0	0.5	24	63.5
9	2	2.0	0.7	24	62.3
10	2	2.0	0.7	12	63.3
11	2	2.0	0.7	24	63.5
12	2	2.0	0.7	36	63.5

Table A6. Ablation study on SPF-DPP hyper-parameters using VSI-Bench.

on VSI-Bench [38] and report the Average Score as the primary metric. Table A6 summarizes the results, where we vary one parameter at a time while keeping the others fixed at their default values ( $\beta = 2, \tau = 2.0, \alpha = 0.5, b = 24$ ).

**Rotation weight  $\beta$ .** The parameter  $\beta$  balances the contribution of rotational differences relative to translational changes in the geometric kernel. As shown in Rows 1–3, setting  $\beta = 2$  yields the best performance (63.5), although the model is relatively robust to changes in this parameter. A lower weight ( $\beta = 1$ ) leads to a slight drop to 62.8, while an overly aggressive weight ( $\beta = 4$ ) results in a marginal decrease to 63.1. This experimental result confirms that  $\beta = 2$  provides the most suitable balance for our setup.

**Heat diffusion scale  $\tau$ .** We analyze the effect of the diffusion scale  $\tau$ , which controls the propagation range of information in the manifold. Rows 4–6 demonstrate a moderate positive correlation between  $\tau$  and synthesis quality. Increasing  $\tau$  from 1.0 to 2.0 improves the score from 62.1 to 63.5. This suggests that a sufficient diffusion scale helps the DPP capture better global coverage, although the performance gain saturates beyond this point.

**Quality mixing weight  $\alpha$ .** The mixing weight  $\alpha$  modulates the trade-off between semantic quality (relevance) and

diversity. The results in Rows 7–9 indicate that the method performs best at  $\alpha = 0.5$  (63.5). Deviating from this value leads to minor performance drops (62.9 at  $\alpha = 0.3$  and 62.3 at  $\alpha = 0.7$ ). This implies that while balance matters, the system remains effective within a reasonable range of  $\alpha$ , avoiding collapse into pure diversity or pure quality maximization.

**Temporal bandwidth  $b$ .** Finally, we examine the temporal bandwidth  $b$ , which determines the sparsity and connectivity of the viewpoint graph. Comparing Rows 10–12, we observe that increasing  $b$  from 12 to 24 brings a performance gain (63.3 to 63.5). However, further increasing  $b$  to 36 results in saturation (63.5). Since  $b = 24$  corresponds to approximately one second of video content (at 24 FPS) and is sufficient to capture local temporal dependencies, we adopt it as a standard setting. Overall, the ablation study confirms that our method is not overly sensitive to precise hyper-parameter tuning.

## D. Prompt

### D.1. System Prompt

#### SYSTEM\_PROMPT

```
You are a helpful assistant.
# Tools
You may call one or more functions to
assist with the user query.
You are provided with function
signatures within <tool_call></
tool_call> XML tags:
<tool_call>
{"type": "function", "function": {"name
": "video_image_sample_tool", "description": "Given camera
parameters in a bird's-eye-view (BEV) coordinate system, this tool
generates a realistic and clear
video frame to assist in answering
the question.", "parameters": {"type": "object", "properties": {"camera": {"type": "array", "items": {"type": "number"}, "minItems": 3, "maxItems": 3, "description": "The
camera parameters as [x1, y1, r], where (x1, y1) represents the
location on the x-axis and y-axis,
and r represents the camera
direction: r=270 faces right, r=90
faces left, r=0 faces up, and r
=180 faces down in the BEV frame
."}}}, "required": ["camera"]}}}
</tool_call>

# How to call a tool
```

Return a JSON object containing the function name and arguments within <tool\_call></tool\_call> XML tags:

```
<tool_call>
{"name": <function-name>, "arguments": <args-json-object>}
</tool_call>

Example:
<tool_call>
{"name": "video_image_sample_tool", "arguments": {"camera": [100, 200, 145]}}
</tool_call>
```

### D.2. User Prompt

#### USER\_PROMPT

Question: {}

Think first. If needed, call video\_image\_sample\_tool to obtain a real and clear video frame, then answer.  
The output format must strictly be: <think>...</think> <tool\_call>...</tool\_call> (if tools are needed) or <think>...</think> <answer>...</answer>